Structure and assembly of the S-layer determine virulence in *C. difficile*

Oishik Banerji
Birkbeck
Paola Lanzoni-Mangutchi
Newcastle University
Filipa Vaz
Oslo University Hospital
Anna Barwinska-Sendra
Newcastle University
Jason Wilson
University of Sheffield https://orcid.org/0000-0002-6967-0809
Joseph Kirk
University of Sheffield
Shauna O'Beirne
University of Sheffield
Arnaud Basle
Newcastle University
Kamel El Omari
Diamond Light Source https://orcid.org/0000-0003-3506-6045
Armin Wagner
Diamond Light Source https://orcid.org/0000-0001-8995-7324
Neil Fairweather
Imperial College London https://orcid.org/0000-0002-3224-0207
Gillian Douce
University of Glasgow
Per Bullough
University of Sheffield https://orcid.org/0000-0001-8147-1127
Robert P Fagan
University of Sheffield https://orcid.org/0000-0002-8704-4828
Paula Salgado (✉ paula.salgado@newcastle.ac.uk)
Newcastle University

Biological Sciences - Article

Keywords: Structure, assembly, S-layer, determine, virulence, C. difficile

Posted Date: October 23rd, 2020

DOI: https://doi.org/10.21203/rs.3.rs-79088/v1

Version of Record: A version of this preprint was published at Nature Communications on February 25th, 2022. See the published version at https://doi.org/10.1038/s41467-022-28196-w.

Abstract

Many bacteria and archaea possess a cell surface layer – S-layer – made of a 2D protein array that covers the entire cell. As the outermost component of the cell envelope, S-layers play crucial roles in many aspects of cell physiology. Importantly, many clinically relevant bacterial pathogens possess a distinct S-layer that forms an initial interface with the host, making it a potential target for development of species-specific antimicrobials. Targeted therapeutics are particularly important for antibiotic resistant pathogens such as *Clostridioides difficile*, the most frequent cause of hospital acquired diarrhea, which relies on disruption of normal microbiota through antibiotic usage. Despite the ubiquity of S-layers, only partial structural information from a very limited number of species is available and their function and organization remains poorly understood. Here we report the first complete atomic level structure and in situ assembly model of an S-layer from a bacterial pathogen and reveal its role in disease severity. SlpA, the main *C. difficile* S-layer protein, assembles through tiling of triangular prisms abutting the cell wall, interlocked by distinct ridges facing the environment. This forms a tightly packed array, unlike the more porous S-layer models previously described. We report that removing one of the SlpA ridge features dramatically reduces disease severity, despite being dispensable for overall SlpA structure and S-layer assembly. Remarkably, the effect on disease severity is independent of toxin production and bacterial colonization within the mouse model of disease. Our work combines X-ray and electron crystallography to reveal a novel S-layer organization in atomic detail, highlighting the need for multiple technical approaches to obtain structural information on these paracrystalline arrays. These data also establish a direct link between specific structural elements of S-layer and virulence for the first time, in a crucial paradigm shift in our understanding of *C. difficile* disease, currently largely attributed to the action of potent toxins. This work highlights the crucial role of S-layers in pathogenicity and the importance of detailed structural information for providing new therapeutic avenues, targeting the S-layer. Understanding the interplay between S-layer and other virulence factors will further enhance our ability to tackle pathogens carrying an S-layer. We anticipate that this work provides a solid basis for development of new, *C. difficile*-specific therapeutics, targeting SlpA structure and S-layer assembly to reduce the healthcare burden of these infections.

Full Text

This preprint is available for download as a PDF.

Figures

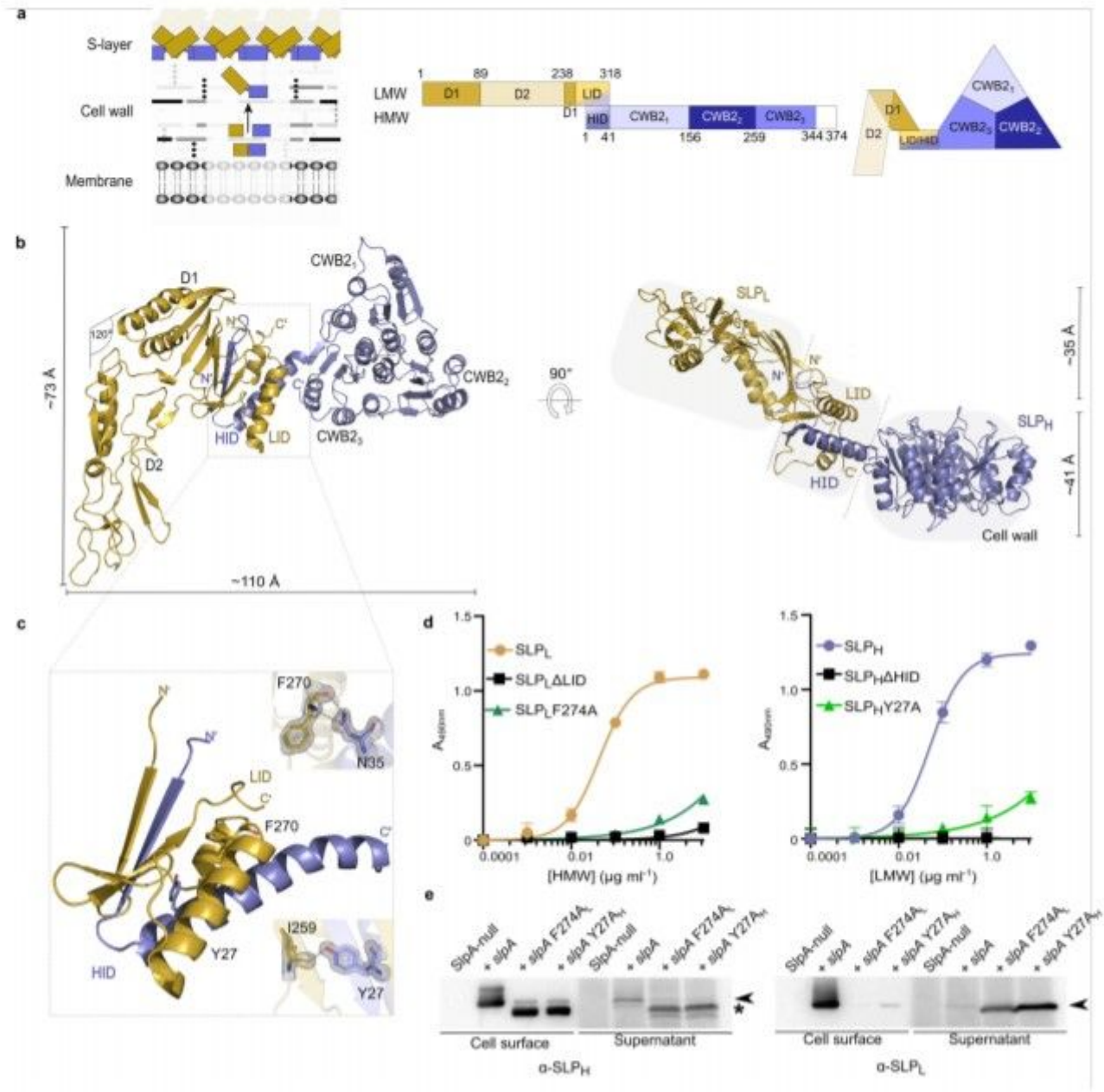

Figure 1

Architecture and key interactions in C. difficile SLPH/SLPL (H/L) complex a, SlpA arrangement on the cell surface (left; SLPL colored in gold and SLPH in slate blue) with detailed organization of protein building blocks in its primary sequence (middle) and quaternary structure (right). Numbering based on the subunits of SlpA from strain CD630, Slayer cassette type 7 (SCLT-7), PBD ID: 7ACY. b, Cartoon representation of H/L complex as viewed from the external environment (top view, left) and side (right). The SLPL protrudes above the SLPH subunit, creating a two-plane arrangement. Three distinct structural features are observed: SLPH, D1 and D2, and LID/HID (regions highlighted in gray). c, 'Paperclip'

organization of the interacting domains LID/HID is maintained by a range of interactions, with selected interface residues identified in strain R7404 (SCLT-7b, PDB ID: 7ACW) depicted as sticks. 2mFo-DFc electron density map is shown on the interacting amino acid pairs as a grey mesh contoured at 1.5 s. Specific interatomic interactions identified with PDBePISA are represented as a dashed line (more details on Extended Data Fig. 2). d, Probing of CD630 H/L complex interactions in vitro with ELISA, comparing effects of intact SLPL (gold circles), SLPH (slate blue circles), variants lacking interacting domains (black squares) and substitution mutants of F274A (structurally equivalent to F270 in R7404 LID/HID depicted in c, dark green triangles) and Y27A (light green triangles) on H/L complex formation. Graphs represent mean ± standard deviation (SD) of n = 3 experiments, with least squares curve fit of product formed upon interaction of the two subunits. e, Western blot of cell surface extracts and culture supernatants, detecting (black arrowhead) SLPH (left) and SLPL (right) in strains devoid of endogenous slpA and expressing plasmid-borne SlpACD630 native protein or variants with either F274AL or Y27AH substitution mutants in SLPL or SLPH (denoted in subscript), respectively. Detected product of partial degradation of HMW indicated with an asterisk.

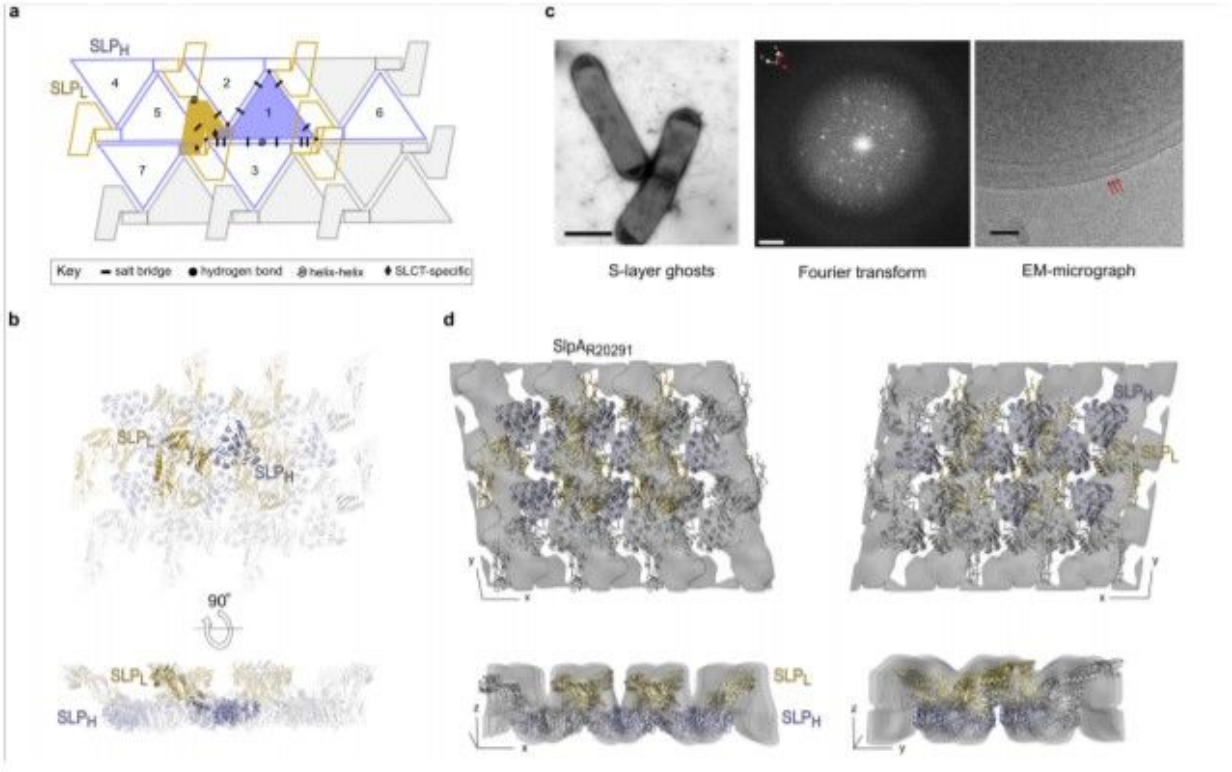

Figure 2

Planar crystal packing in the X-ray structure fits the in situ packing of the native Slayer a, 2D schematic of H/L complex crystal packing, indicating the interaction network linking a single SLPL (gold)/ SLPH (slate blue) complex with six other molecules in a planar arrangement generated by SLPH tiling. Array is

depicted as seen from the extracellular environment, with symbols representing key interaction types in the crystal lattice, shown in detail in Extended Data Fig. 4. b, Cartoon representation of the H/L planar array (PDB ID 7ACY, colored as in a, views as defined in Fig. 1b). c, Native C. difficile S-layer ghosts (electron micrograph, negatively stained, left. Scale bar: 2 μm) were used to compute Fourier transforms (middle). Typically spots from two or more lattices were observed. Reciprocal lattice axes (red and white axes) are indicated for two observed lattices (scale bar 0.0125 Å-1). Intact frozen hydrated C. difficile cells, examined by cryo-electron microscopy (right), show distinctive ridged surface indicated by red arrows (scale bar 50 nm). d, Orthogonal views of the 3D reconstruction of negatively stained S-layer ghost indicating the overall envelope in the native lattice. A rigid body fit of the structure of H/L complex determined by X-ray crystallography (PDB ID: 7ACY, cartoon representation, SLPL - gold, SLPH - slate) indicates a similar arrangement in the native S-layer ghosts and crystal packing. Reconstruction is shown from the environment (top left) and cell wall (top right), and side views in the 2D plane (bottom panels).

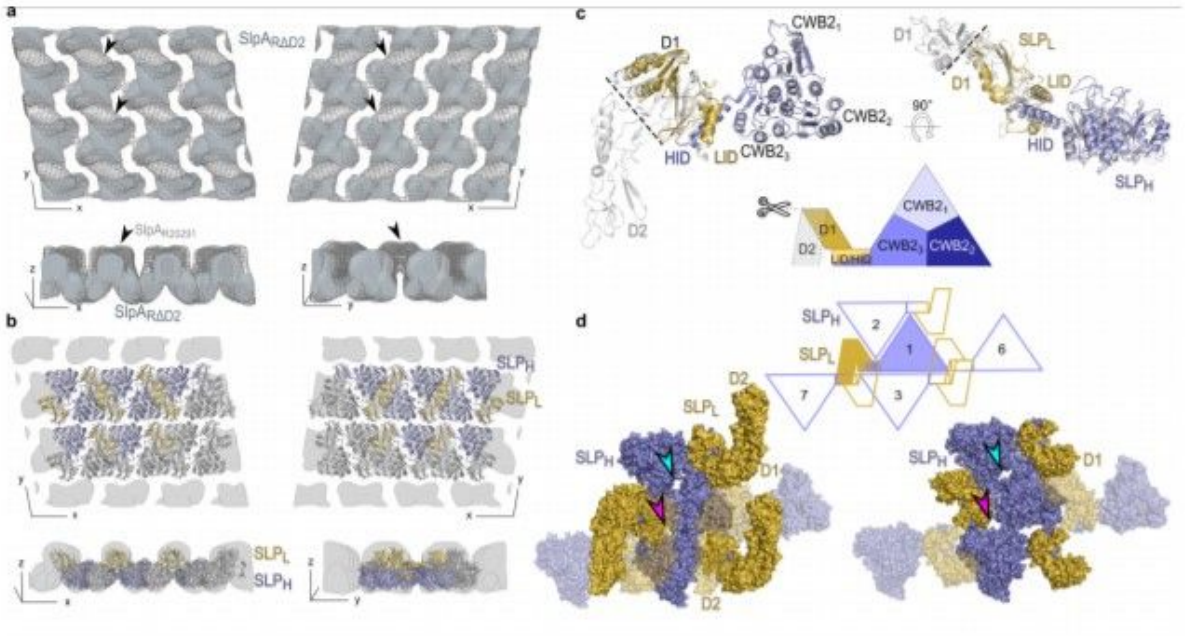

Figure 3

The flexible D2 domain is dispensable for S-layer assembly a, Superimposition of the 3D reconstruction of negatively stained S-layer ghost containing SlpA devoid of domain D2 (SlpARΔD2, light blue solid surface) on the reconstruction of native wild type S-layer ghost (SlpAR20291, grey mesh). The missing density can be largely ascribed to that of the missing D2 domain (indicated with black arrowheads). Views are as described in Fig. 2d. b, Fit of the SlpARΔD2 structure determined by X-ray crystallography (colored as in c) into the S-layer (gray) reconstruction indicates a similar arrangement in the crystal packing and the native array. Views as in a. c, Cartoon representation of the SlpARΔD2 H/L complex crystal structure (slate blue and gold, PDB ID: 7ACZ), superimposed onto SlpACD630 H/L complex

structure (PDB ID: 7ACY, gray). Deleted D2 region is marked with a dashed line on the CD630 structure and corresponding schematic representation of the complex. Views as in Fig. 1b. d, Surface representation of wild type H/L (7ACY, left) and SlpARΔD2 H/L(7ACZ, right) crystal packing showing pores in the 3D crystal lattice (top). Positions of pores marked with arrowheads (pore 1 in magenta, pore 2 in cyan) are equivalent in both lattices.

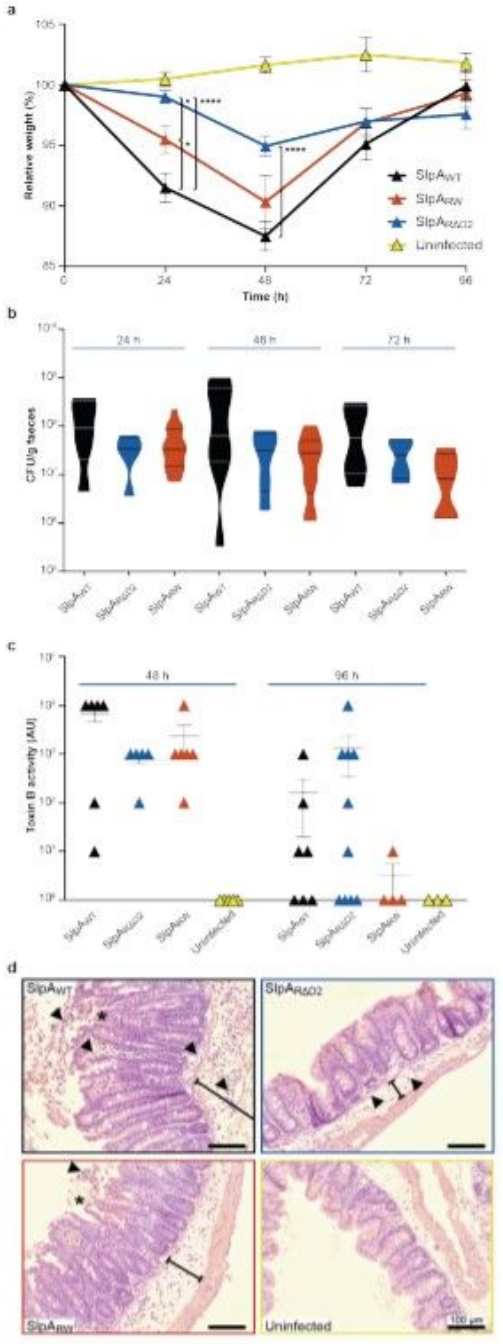

Figure 4

In vivo evaluation of C. difficile strains producing a modified S-layer a, Relative percentage weight loss of antibiotic-treated animals infected with R20291 (SlpAWT, black triangle), RΔD2 (SlpARΔD2, blue triangle), FM2.5RW (SlpARW, orange triangle) and antibiotic-treated uninfected animals (Uninfected, yellow triangle). b, Total C. difficile counts (CFU ml-1) recovered from faeces at 24, 48 and 72h post infection. c, Measurement of toxin activity in filtered caecal extracts from individual animals. Annotations as in a. d, Hematoxylin and eosin stained caecal histological sections from animals 48 h post infection with C. difficile, representing acute disease. Arrowheads highlight the margination and tissue infiltration of polymorphonuclear cells (PMNs) and the breached epithelial barrier (indicated with asterisk). The extent of tissue edema between basal membrane and musculature is highlighted (line). Crypt hyperplasia is discernible in tissue from R20291 (SlpAWT) and FM2.5RW (SlpARW) infected animals, compared to antibiotic-treated uninfected animals or those infected with RDD2 (SlpARΔD2). Data analysis represents a total of up to 15 mice per strain tested from 3 experiments expressed as mean (± SEM) a (10-15 mice), c (5 mice); or as violin plots showing medians (solid lines), upper and lower quartile (dashed line) and max/min range (top and base of the plot) b, (min 5 mice). Non-parametric, non-paired Mann-Whitney statistical tests were performed with differences of *p = <0.05, ****p = <0.0001 indicated (a, c). Scale bars of 100mm are shown (d).

Supplementary Files

This is a list of supplementary files associated with this preprint. Click to download.

- SIdataalignmentSlayer.pdf
- SImovieSlayer.mp4
- SIguideSlayer.pdf
- SIdiscussionSlayer.pdf
- SIdataalignmentSlayer.pdf
- SITable1.pdf
- SITables23.pdf
- MethodsSlayer.pdf